ELSEVIER

Available online at www.sciencedirect.com
SCIENCE DIRECT®

Computational Materials Science 33 (2005) 92–105

COMPUTATIONAL MATERIALS SCIENCE

www.elsevier.com/locate/commatsci

Atomistic modeling of dopant implantation and annealing in Si: damage evolution, dopant diffusion and activation

Lourdes Pelaz *, Luis A. Marqués, Maria Aboy, Pedro López, Juan Barbolla

Department Electricidad y Electronica, ETSI Telecommunication, Campus Miguel Delibes, University of Valladolid, E-47011 Valladolid, Spain

Abstract

In this paper we discuss some of the issues involved in the modeling of damage evolution, dopant diffusion and electrical activation as a result of ion implantation and annealing processes in Si. Dopant diffusion and activation during thermal anneal is complicated by the presence of the damage generated by the energetic impinging ion. Of particular interest is the case of B, as it is the most common dopant used for the formation of p+ junctions. We review the correlation between defect evolution and B diffusion and B clusters, both for sub-amorphizing and amorphizing implants. The effects of implant parameters and annealing conditions will be analyzed. Although we concentrate on Monte Carlo modeling, links to more detailed ab initio and molecular dynamics simulations as well as continuum modeling and experiments complement this analysis.
© 2004 Elsevier B.V. All rights reserved.

PACS: 61.80.Az; 82.20.Wt; 67.80.Mg; 61.72.Ji
Keywords: Modeling; Silicon; Defects; Boron

1. Introduction

Ion implantation is the most common method of introducing dopant atoms for the fabrication of Si devices. This process provides excellent spatial and dose control, as well as ease of manufacture. As the energetic ions are introduced in the Si lattice, many Si atoms are knocked off their lattice positions resulting in large numbers of Si interstitial atoms and vacant lattice sites (Frenkel pairs). Since the as-implanted dopants are usually electrically non-active and the lattice damage deteriorates the device performance, it is necessary to have the annealing of the implanted sample at temperatures high enough to permit the dopant atoms to incorporate into substitutional sites and thus

* Corresponding author. Tel.: +34 983 423683x5502; fax: +34 983 423675.
E-mail address: lourdes@ele.uva.es (L. Pelaz).

0927-0256/$ - see front matter © 2004 Elsevier B.V. All rights reserved.
doi:10.1016/j.commatsci.2004.12.043

become electrically active, and for the defects to annihilate and thus repair the damage.

The diffusion of impurities in implanted Si during thermal anneal is complicated as a result of the presence of implantation damage. As an example, the diffusivity of B in implanted crystalline Si is anomalously high compared to equilibrium values [1]. This phenomenon has important consequences for Si processing, since it causes the dopant profile to spread significantly compared to the as-implanted profile during the subsequent annealing steps required for dopant activation. The presence of damage also causes dopant clustering and thus prevents complete electrical activation. The down-scaling of Si CMOS devices requires simultaneously the formation of ultrashallow junctions for the source and drain extensions and a low sheet resistance (high carrier concentration) [2]. Conventionally, there is a compromise involved in maximizing dopant electrical activation while minimizing dopant diffusion.

Implantation induced damage ranges from single point defects and defects clusters in crystalline silicon, to the formation of amorphous pockets and even continuous amorphous layers if the implant dose is high enough. The understanding of the damage generation and dissolution is of great relevance because its interaction with dopants defines the final carrier profiles. In addition, the implant damage itself may degrade the carrier mobility and may act as generation centers that induce excessive leakage current. Therefore, the junction depletion region should be far away from any residual damage or this must be completely annealed. A highly damaged region that does not form a continuous amorphous layer requires annealing temperatures of 800–1000 °C to remove extended defects and to place all of the implanted ions into substitutional positions, which is accompanied by significant dopant diffusion. The formation of the amorphous phase is beneficial because it not only limits ion channeling (which can distort the implanted dopant profile) but it is easily annealed. Annealing, which occurs by solid phase epitaxial growth (SPEG) [3], results in the incorporation of the dopants into electrically active positions during the low temperature regrowth (550–650 °C) [4] and in a low defect density in the recrystallized volume [5]. After SPEG only the residual defects beyond the amorphous–crystalline (a/c) interface remain and require higher temperatures for their complete dissolution. SPEG of preamorphizing implants appears to be a promising method to achieve high dopant activation with minimal diffusion and thus meet the performance specification of the 65 and 45 nm node [6]. However, if the dopant concentrations are very high ($\sim 10^{21}$ cm^{-3}), SPEG only gives active concentrations up to $\sim 3 \times 10^{20}$ cm^{-3}. This activation level appears to be metastable and more deactivation occurs during additional annealing steps [7].

Since the cost of test lots of Si devices is too expensive, the development of physics-based models that properly describe defect evolution and dopant-defects interactions, and their implementation in process simulators, have become an essential step for device optimization. A multiscale modeling is needed to describe dopant and defect interactions at atomic scale and at the same time to provide macroscopic dopant profiles [8].

In this paper we analyze the physical models that describe ion implantation damage and the interactions between defects and B. Calculations based on molecular dynamics (MD), kinetic Monte Carlo (KMC) as well as continuum methods are linked to provide an atomistic insight in the problem, at the same time that the results can be extended to macroscopic scales directly comparable to experiments.

2. Simulation techniques

Analytical descriptions based on linear Boltzmann transport theory, [9] and computer simulation codes, such as TRIM [10] and MARLOWE [11] based on the binary collision approximation (BCA) [12], are used to provide a description of the implanted ion profile and the generated damage. MD simulation methods can be used to treat the full dynamics of the collision process [13–15] and to predict the formation of realistic damage microstructures not accessible to BCA-based calculations. This technique also permits to simulate the annealing of the damage. However, due to the extensive computer load only small sizes ($<10^6$ lattice atoms) and times ($\sim$nanoseconds)

are feasible with this technique. Atomistic KMC computer codes [16–18] and continuum methods [19,20] extend spatial and temporal scales and provide results directly comparable to experiments.

Unlike MD simulations, KMC computer codes do not simulate the vibrational movement of the Si atoms in the lattice, and only the dynamics of defects (diffusion, emission from clusters, recombination...) is followed. Parameters that define these atomic interactions, such as diffusivities, binding energies, capture radius, etc, are derived from ab initio [21–26] and MD [13] calculations, or dedicated experiments [17,18]. The time step is variable and it may go from 10^{-9} s for fast diffusing species, to 10^{-3} s or even longer, for the emission of defects from stable clusters. Generally, fast events tend to disappear quickly, leaving slower events that raise the time step.

As an example, we will consider the Si interstitial clustering evolution, which can be written as a chemical reaction between a mobile free interstitial, I, and an interstitial cluster with m interstitials, $C_{(m)}$, to result in an interstitial cluster with $m + 1$ interstitials, $C_{(m+1)}$

$$I + C_{(m)} \leftrightarrow C_{(m+1)}. \qquad (1)$$

In KMC methods chemical reactions are associated to particle interactions and events. In this example, a Si interstitial in a cluster can be emitted (event) or can interact with a free Si interstitial and capture it (interaction). A free Si interstitial can experience diffusion hops (event) or interact with an interstitial cluster and be captured. Events are characterized by the emission or jump frequencies, and interactions by the capture radius. The total event rate, R, of a system with n free Si interstitials and m Si interstitials in clusters is

$$R = n \cdot \frac{6D_{\mathrm{I}}}{(\beta a)^2} + m \cdot \frac{6D_{\mathrm{I}}}{(\beta a)^2} \exp\left(\frac{-E^{\mathrm{I}}_{\mathrm{bind}}}{k_{\mathrm{B}}T}\right). \qquad (2)$$

where D_{I} is the Si interstitial diffusivity, $E^{\mathrm{I}}_{\mathrm{bind}}$ the binding energy of the Si interstitial to the cluster, βa hop distance in terms of the silicon lattice spacing, a, k_{B} the Boltzmann constant, and T the temperature.

A random number ($0 < rn1 < R$) determines the event: a diffusion hop or the interstitial emission from a cluster. Depending on the selected event, another random number ($0 < rn2 < n$, or $0 < rn2 < m$) chooses the particular interstitial that experiences the event. An additional random number gives the direction of the jump (or emission) to a distance βa. When the selected particle is moved to a new position, its neighbors are checked for possible interactions. The neighbors are defined as particles that lie within the capture radius, αa, of a given particle. If, for instance, a free interstitial experiences a diffusion hop and lies within the capture radius of an interstitial cluster, the free interstitial disappears and becomes part of the cluster. Then, the total event rate must be updated to

$$R = (n-1) \cdot \frac{6D_{\mathrm{I}}}{(\beta a)^2} + (m+1) \cdot \frac{6D_{\mathrm{I}}}{(\beta a)^2} \exp\left(\frac{-E^{\mathrm{I}}_{\mathrm{bind}}}{k_{\mathrm{B}}T}\right). \qquad (3)$$

The simulation of an event increases the time by an amount $\Delta t = 1/R$ and the scheme is repeated until the specified time is reached. The time step is mostly determined by the faster event. The frequency associated to diffusion events is many orders of magnitude higher than that associated to the emission of interstitials from clusters. For example, at 800 °C, if we take $D_{\mathrm{I}} = 10^{-6}$ cm^2 s^{-1}, $\beta a = 3.84$ Å, and $E^{\mathrm{I}}_{\mathrm{bind}} = 2.6$ eV, the diffusion frequency is $\sim 10^9$ s^{-1}, while the emission frequency is 12 orders of magnitude slower. The time step for each diffusion event is very small ($<10^{-9}$ s) and a huge amount ($>10^9$) of these events should be simulated for the time to advance one second. On average, the faster event will be selected orders of magnitude more often than the slower event. This means that free interstitials are very likely to be selected, experience diffusion hops and be captured before any of the interstitials in clusters are emitted. The system thus ends up with $(n + m)$ interstitials trapped in clusters. In that instant, the emission of an interstitial form a cluster is the only possible event, which gives a time step 12 orders of magnitude higher than that associated with diffusion events. This increase in the time step makes the simulation of actual process times possible. Since particles are chosen randomly according to their event rates, a large number of particles

must be included in the simulation cell to reduce the statistical error. However, with the computer power available nowadays, hundreds of thousands of particles can be easily traced.

In continuum process simulators the physics of the system is formulated as a series of differential equations for each particle type. Typically they are continuity equations, where each particle gain or loss is formulated in terms of its generation and recombination rates and the diffusion flux [27]. The reaction rates are defined according to the parameters that characterize the interaction, and are the same as in KMC. The numerical solution of these set of non-linear partial differential equations requires the spatial and temporal discretization to reduce the derivatives into algebraic differences. The problem is converted to a large, non-linear system of coupled equations, which are solved using standard numerical methods. In principle, continuum methods can be used to define the same defect and dopant interactions as KMC codes [8].

Continuing with the same example, the rate of change of the clustered Si interstitial concentration, C_C, and that of the free Si interstitial concentration, C_I, can be formulated in terms of the Si interstitial cluster growth and dissolution rates through the capture and emission of free interstitials. The equation for free Si interstitials also includes the gradient of the flux, as free interstitials are mobile

$$\frac{\partial C_C}{\partial t} = 4\pi\frac{\alpha^3}{\beta^2}a \cdot D_I \cdot C_C \cdot C_I - \frac{6D_I}{(\beta a)^2}\exp\left(\frac{-E^I_{bind}}{k_B T}\right) \cdot C_C, \quad (4)$$

$$\frac{\partial C_I}{\partial t} = \nabla(D_I \cdot \nabla C_I) - 4\pi\frac{\alpha^3}{\beta^2}a \cdot D_I \cdot C_C \cdot C_I + \frac{6D_I}{(\beta a)^2}\exp\left(\frac{-E_{bind}}{k_B T}\right) \cdot C_C. \quad (5)$$

If other defects, such as vacancies, dopants or traps were considered, similar equations to those for Si interstitials should be formulated for each of them. In addition, coupling terms corresponding to interstitial–vacancy or dopant-interstitial interactions should be added to the differential equations, which make their resolution more difficult. In KMC methods additional reactions only require new event rates to be added to the total event rate, and the proper definition of the capture radius of the interactions. Thus new reactions hardly add any computational load. The main difficulty arises from the determination of the new parameters (binding energies, diffusivities, capture radius) that describe the interactions, but this is also necessary in continuum methods. The efficiency of continuum methods lies on the use of simplified models that reduce the number of equations to be solved simultaneously. This technique is generally faster and allows simulations of big sizes by adjusting the grid size used for the spatial discretization. However, this advantage is reduced as the device size shrinks and complex physical interactions need to be modeled. The use of a very refined grid and a large number of equations slow down the resolution of the problem using continuum methods. In those cases, KMC can be advantageous.

When analyzing ion implantation and diffusion, a significant difference between continuum and atomistic process simulators comes from the spatial correlation between defects in the cascade. While atomistic models take into account the actual positions of Frenkel pairs generated by BCA or MD codes, continuous simulators usually take the average defect profile. Implant cascades produce high defect density zones separated by regions of undamaged crystal. This kind of defect distribution clearly differs from a uniform defect profile in the whole implanted region. The difference is more obvious for low dose implants because of the larger separation between cascades. Hobler et al. [28] analytically considered the correlation between defect positions in order to be able to include this effect in continuum methods. For high doses, cascades overlap and it is not possible to distinguish the damage of different cascades.

3. Damage generation and annealing

Damage produced by implantation is generally described by the distribution of displaced atoms

or Frenkel pairs along the collision cascade generated by the incoming ion. MD simulations reveal that extended amorphous regions can be directly formed during the collision cascade [14,15]. Depending on the temperature, disordered regions or displaced atoms may remain or they can rearrange and recover the lattice. The mechanisms by which damage accumulates and may eventually lead to amorphization have been subject of intense debate. Some authors propose that amorphization occurs homogeneously by the accumulation of uniformly distributed point defects above certain threshold value [29]. Other authors suggest that the overlap of these amorphous regions causes the heterogeneous nucleation of the amorphous phase [30].

Recently, a new atomistic amorphization model implemented in KMC code has been proposed. It conciliates both theories and reproduces quantitatively many of the experimental findings [31]. In addition to Si interstitials and vacancies, the model uses the defect known as IV pair or bond defect to describe implantation damage in Si [32,33]. The IV pair consist of a local rearrangement of the bonds in the Si lattice with not excess or deficit of atoms. Tigh binding simulations showed that this defect could form by incomplete interstitial–vacancy recombination [34]. Other theoretical studies revealed that the defect can be formed as well during the ballistic process of the cascade [35]. Although MD calculations indicate that the isolated IV pair within a perfect crystal Si is unstable at room temperature, the agglomeration of these defects produce more stable structures that are assimilated to amorphous pockets. Marqués et al. [32] have shown that amorphous Si can be described by the accumulation of a sufficiently high concentration (>25%) of IV pairs. The rate of recombination of each IV pair is determined by the number of IV neighbors. This local characterization explains many of the observed features in the annealing behaviour of amorphous pockets [33] and the kinetic of damage accumulation [31]. Since the IV pair defect contains no excess or deficit of atoms, when it annihilates no net point defects are released to the lattice. However, MD simulations show that amorphous pockets generated by ion implantation frequently contain an excess or deficit of atoms compared to the perfect crystal. When amorphous regions completely regrow these unbalanced atoms are left behind as ordinary Si self-interstitials or vacancies [14].

3.1. Sub-amorphizing implants

Small amorphous pockets may be formed even in implants that do no cause the formation of continuous amorphous layers [15]. After the regrowth of disconnected amorphous pockets, local clusters of Si self-interstitials and vacancies are formed in the implanted region. The emission of point defects from these clusters and its diffusion lead to further formation of IV pairs that quickly annihilate. Only the excess defects that have not partner to recombine with, remain. Si interstitials and vacancies are generated in pairs, but since the implanted ion generally sits in a substitutional position, one Si self-interstitial per implanted ion is generated in excess over the number of vacancies. Therefore, in spite of the complexity of the generated damage, the "effective" damage consists of an Si self-interstitial profile that mirrors that of the implanted ion. This is the basis of the "+1 model" proposed by Giles to model defects and dopant diffusion in continuum simulators [36]. Detailed KMC simulations provided the understanding and justification for this model [16]. In Fig. 1 we show the evolution of the implant damage and the interstitial diffusing hops, taking into account all the Frenkel pairs, and using the +1 model. As we can see, the level and duration of the residual damage as well as the total number of diffusion hops are similar in both cases.

More detailed studies on the damage distribution have shown that some corrections to the "+1 model" may be needed [37–39]. For the "+1" model to be valid is necessary that Si self-interstitials and vacancies are sufficiently close so that the probability of recombination is much higher than that of interaction with dopants. However, this is not always the case. For example, the large momentum transfer to lattice atoms by heavy ions causes a net displacement of Si interstitials compared to the corresponding vacancy sites. This spatial separation between Frenkel pairs makes their recombination more difficult. The result after

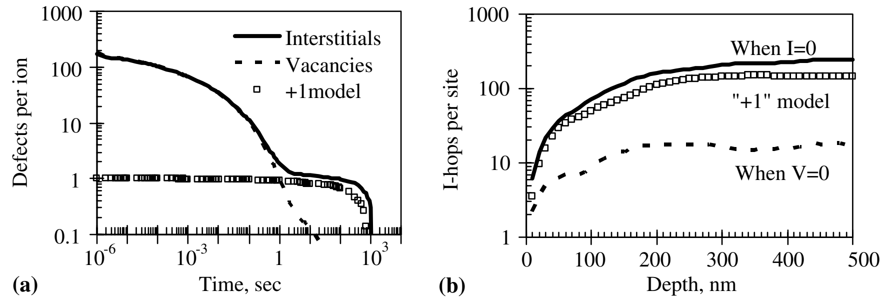

Fig. 1. (a) Time evolution of the total number of Si self-interstitials and vacancies and (b) Si interstitial hops, corresponding to a 150 keV Si implant to a dose of 7×10^{13} cm^{-2}, annealed at 800 °C. The number of hops given until the vacancies have disappeared (when $V = 0$) is negligible compared to the number of hops given until all the Si insterstitials have disappeared (when $I = 0$). This number is similar to the one obtained using the "+1 model".

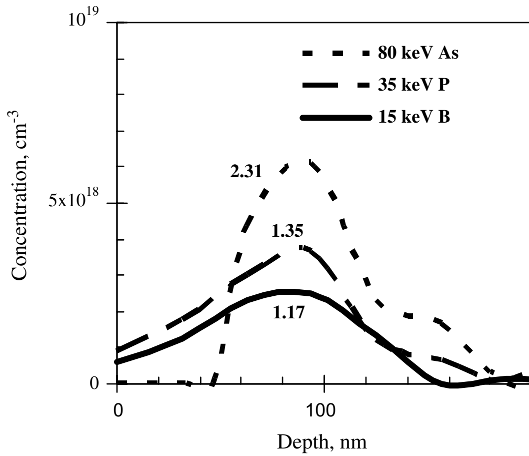

Fig. 2. Si interstitial profile after Frenkel pair recombination for B, P and As implants of similar projected range. The numbers near the profiles are the "+n" interstitials per implanted ion that survive to recombination.

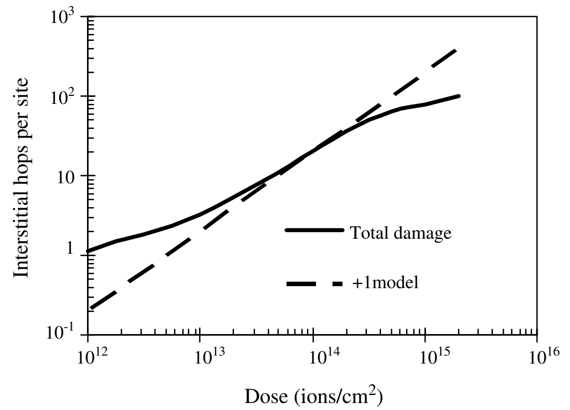

Fig. 3. Time integrated Si interstitial hops per lattice site as a function of the implanted dose for a 10 keV Si implant after all the excess Si interstitials have been annihilated. The dashed line correspond to the simulation using the "+1" model and the solid line correspond to the simulation using the total damage produced in the implantation cascade.

local recombination is a shallow vacancy profile separated from the deeper Si self-interstitial profile [37]. The number of surviving Si interstitials is thus higher than the number of implanted ions and increases with the ion mass, as we can see in Fig. 2.

Another interesting example that reveals the limitation of the +1 model occurs for low dose implants [38]. In this case, the spacing among implant cascades prevents inter-cascade interactions, which results in an incomplete Frenkel pair recombination. A similar effect occurs for high implant temperatures because the dynamic anneal of each cascade prevents their interaction. Fig. 3 shows the average number of interstitial hops per lattice site vs. dose using the "+1" model and considering all the damage generated in the cascades. In the "+1" model the number of Si interstitials equals to the dose, and so the number of hops increases linearly with dose. For low doses, the total number of interstitial hops in the case of complete damage, is significantly higher than that for the "+1" model. As the dose increases and cascades overlap, interstitials and vacancies even from different cascades are so close that they recombine with a negligible number of hops. Thus the number of interstitials hops approaches the value

corresponding to the "+1" model. For amorphizing doses, the effective damage is lower than the implanted dose, as we shall explain later.

3.2. Amorphizing implants

During the regrowth of a continuous amorphous layer, Si or dopant atoms are placed into lattice positions. Any excess or deficit of atoms is swept as the a/c interface advances. When the amorphous layer extends to the surface, the unbalanced atoms are adjusted there. Thus, after SPEG, the amorphous layer is free of defects [5]. If the amorphous layer is buried, a band of defects is formed where the two regrowing interfaces merge [40]. In both cases, defects beyond the a/c interface evolve in a similar fashion as those in highly damaged but sub-amorphizing implants: the net excess defects in that region survive. In this case only the fraction of the "+n" interstitial profile beyond the a/c interface can be considered as an initial condition for continuum simulators [41]. In Fig. 4, we show the residual damage for sub-amorphizing and amorphizing implants after a short anneal at 550 °C, enough to regrow the amorphous regions. While the residual damage in the sub-amorphizing implant is similar to the implanted ion profile, only the damage beyond the a/c interface remains after SPEG of the amorphous layer.

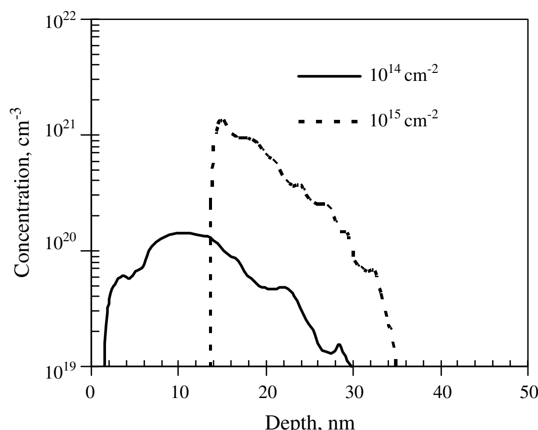

Fig. 4. Residual damage profile after a 200 s anneal at 550 °C for 5 keV Si implants to doses of 10^{14} and $10^{15}\ cm^{-2}$. The lowest dose corresponds to a sub-amorphizing implant. The highest dose produces a continuous amorphous layer up to 14 nm.

Traditionally, amorphization was modeled by assuming that the lattice turns amorphous when a critical point defect concentration was exceeded [29,42]. The total defect profile is generally taken from TRIM or BCA codes, and the threshold concentration value for amorphization is taken by comparing the simulated profile with experimentally measured amorphous layer thickness [43]. One of the main limitations of this simplistic model is the uncertainty in the critical point defect concentration value. Different authors have reported values ranging between 10^{21} and $10^{23}\ cm^{-3}$ depending on implant parameters (see Ref. [42] and references therein). Although this uncertainty leads to variations of only a few nanometers in the predicted depth of the a/c interface, the residual damage beyond it may change up to 50% because the region near the a/c interface contains the larger defect concentration. Variations in the critical defect concentration account for changes in the amount of retained defects compared to the generated damage. The resistance of the damage to anneal depends on implant parameters (ion mass, substrate temperature...) thus explaining the variations of the critical defect concentration.

MD simulations have shown that heavy ions generate large amorphous pockets more resistant to anneal than small damage clusters produced by light ions [15]. In our damage model, the rate of recombination of IV pairs is lower as they are surrounded by more IV pairs [33]. This accounts for the faster recombination of dilute damage compared to dense structures. In the model, we also consider the substrate temperature and the dose rate by performing the appropriate anneal during the implant process. Thus, the position of the a/c interface and the residual damage vary with implant parameters.

3.3. Defect evolution

After IV recombination of small amorphous pockets or SPEG of a continuous amorphous layer, residual interstitials agglomerate into defect clusters and extended defects. Their dissolution in-

jects Si interstitials that may interact with dopants and cause excessive dopant diffusion and clustering [1,17,18]. A number of theoretical calculations [13,44] and experiments [45,46] have been used to evaluate their energetics, identify their nature and monitor their evolution. MD calculations have shown that the migration barrier for Si self-interstitials is in the order of 1 eV [13]. Although some authors have suggested that the di-interstitial may have also a large mobility [13,47], it has been demonstrated that this feature is not relevant for defect evolution and dopant diffusion [47]. Therefore, we will consider that only free Si interstitials and vacancies, and not their clusters, are mobile. For implant doses higher than 10^{13} cm^{-2}, Si interstitials mostly condense into rod-like defects in the [1 1 3] plane, whose activation energy was obtained to be ~3.6 eV by TEM measurements [45]. For amorphizing implants, dislocation loops are formed with the residual Si-interstitial damage beyond the a/c interface [48]. The formation energies of these defects, or equivalently, their binding energies, are relevant parameters in process modeling since they determine the emission rate of Si interstitials from the defects, and thus define their dissolution time and the Si interstitial supersaturation.

Some interesting magnitudes can be obtained from the differential equations that describe Si interstitial clustering (Eqs. (4) and (5)) [27]. Assuming that Si interstitials are in equilibrium with their clusters ($\partial C/\partial t = 0$ in Eq. (4)), the Si interstitial concentration in the defect band, located at a distance R_p from the surface, can be written as

$$C_I = \frac{6}{4\pi(\alpha a)^3} \exp\left(-\frac{E^I_{bind}}{k_B T}\right). \qquad (6)$$

Assuming that C_I is maintained constant until the Si interstitial clusters disappear, the flux of Si interstitials to the surface is given by $\sim D_I C_I / R_p$. The integral of this flux until all clusters disappear is equal to the total dose of Si interstitials stored in Si interstitial clusters (which is equal to the implanted dose, Φ, according to the +1 model). Therefore, the duration of the clusters is given by

$$\tau = \frac{\Phi \cdot R_p}{D_I C_I} = \frac{\Phi \cdot R_p}{D_{I0} C_{I0}} \exp\left(\frac{(E^I_m + E^I_{bind})}{k_B T}\right), \qquad (7)$$

where D_{I0} and C_{I0} are the prefactors for the interstitial diffusivity and the interstitial concentration, and E^I_m is the migration barrier of the Si self-interstitial.

Si interstitial defects follow a non-conservative Ostwald ripening, driven by the increasing binding energies and capture radius with increasing defect size. Interstitials released from clusters randomly diffuse and can be recaptured by the same or by other clusters. Thus, there is a continuous exchange of Si interstitials among clusters. Since larger and more stable clusters capture Si interstitials more efficiently and emit them at a slower rate, the net effect is that they grow at the expense of less stable clusters. Fig. 5 shows the results of a KMC simulation for Si-interstitial defects generated by a 40 keV Si implant to a dose of 10^{14} cm^{-2}, during a post-implant anneal at 750 °C. At the very early stages of the annealing, the high Si-interstitial and vacancy concentrations generated by the implantation recombine quickly, leaving approximately one Si interstitial per implanted ion (~10^{14} cm^{-2}). As the anneal proceeds, the remaining interstitials condense into small interstitial clusters and evolve toward larger and more stable defects. While there are many small defects and the distance among them is much

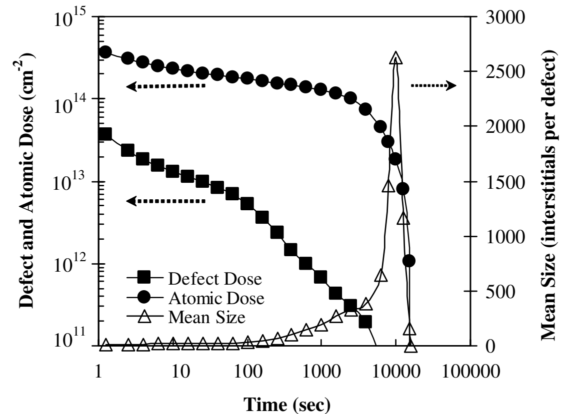

Fig. 5. Time evolution during annealing at 750 °C of the atomic (number of Si interstitials per cm^2) and defect (number of defects per cm^2) dose of Si interstitials in defects for a simulated 40 keV Si implant to a dose of 10^{14} cm^{-2}. The mean size of the defects (number of Si interstitials/number of interstitial defects) is also plotted.

shorter than the distance to the surface, Si interstitials emitted from clusters are more likely to be recaptured by other defects than to reach the surface [49]. Thus, the total number of Si interstitials in clusters remains almost constant, at the same time than the mean size of the defects increases and the number of defects decreases (*Interstitial_dose* = *Defect_dose* × *Average_defect_size*).

When most of the Si interstitials are stored in a few defects of large size, the average distance among defects, which is inversely proportional to the square root of the defect_dose ($d \alpha (Defect_density)^{-1/2}$), becomes comparable to the distance to the surface, R_p. Then, the probability of Si interstitials being recaptured by other defect becomes comparable to the probability of them being annihilated at the surface. Then, a significant number of Si interstitials emitted from clusters are lost by recombination at the surface. Thus the Si interstitial and the defect dose decrease, with the subsequent increase in the distance among defects. Consequently, the probability of interstitials being annihilated at the surface increases further, resulting in the quick dissolution of Si interstitial defects at the final stages of the anneal.

As the implant energy increases and defects are placed deeper, they remain longer time and grow to larger sizes before they dissolve. Analogously, if the implant dose increases, the number of initial Si interstitials is larger, and so the defect density is. Therefore, the average distance among defects is smaller and they can easily be recaptured by other defects favouring their growth. The formation of large defects involves more exchange of Si interstitial among defects, and thus a large probability of the Si interstitials interacting with dopants. The use of ultra-low energy implants for the formation of ultra-shallow junctions has reduced the distance of the defects to the surface and thus defects annihilate quickly. However, when at the same time that low energies high doses are used, big and stable Si interstitial defects appear near the surface [50].

4. Dopant-defects interactions

The damage generated by ion implantation enhances the diffusivity of dopant atoms and can also form defect-dopant complexes that prevent the electrical dopant activation. Dopants that diffuse by an interstitial or interstitialcy mechanism are particularly sensitive to the effect of implant damage, since the residual damage after Frenkel pair recombination consists mostly of Si interstitial defects. This is the case of B, the dopant commonly used to form p-type Si.

4.1. Dopant diffusion

Experiments [51] and theoretical calculations [52,21–24] have demonstrated that the interstitial fraction for B diffusion is close to 1 [1]. B atoms are very weakly bound to vacancy sites [52], while they have a strong binding energy to Si interstitial atoms [21–24]. Some authors describe the B-Si interstitial interaction in terms of pairing and kick-out mechanisms [21], while other calculations show that the Si and B atoms diffuse together as a pair until the B atom occupies the substitutional position and the Si interstitial moves away [22–24]. In terms of modeling both approaches are similar, and the process can be described as a reaction between a substitutional B atom (Bs) and an Si interstitial (I) to generate a mobile B–I pair or interstitial B (Bi):

$$\mathrm{Bs} + \mathrm{I} \leftrightarrow \mathrm{Bi}. \tag{8}$$

Assuming equilibrium between B (C_B) and Si interstitial (C_I) concentrations, the B diffusivity can be written as [53]

$$D_B = D_{Bi} \cdot C_I \exp\left(\frac{E_{bind}^{Bi}}{k_B T}\right), \tag{9}$$

where D_{Bi} is the diffusivity of Bi, and E_{bind}^{Bi} the binding energy between the B and I atoms. Thus, the B diffusivity enhancement D_B/D_B^*, (being D_B^* the equilibrium value) equals to the supersaturation of Si interstitials (C_I/C_I^*). The excess Si interstitials generated in the implantation process quickly condense into Si interstitial clusters. They slowly release Si interstitials setting a C_I, given by Eq. (6), responsible for the enhancement of the B diffusivity. Since Si interstitial clusters eventually dissolve (in the time given by Eq. (7)) and the Si interstitial concentration reaches its equilibrium value, the diffusivity enhancement is a

transient effect. Hence, the name of transient enhanced diffusion (TED) used to describe this effect. The more stable the Si interstitial clusters (larger $E^{\mathrm{I}}_{\mathrm{bind}}$), the lower the enhancement and the longer the duration of TED.

From an atomistic point of view TED is proportional to the number of times that a Si interstitial visits a lattice position and it can thus interact with a dopant atom in that position. From the random-walk theory [54], the average number of hops, N, of a Si interstitial in its way to the surface, only depends on the distance to the surface, R_{p}, and on the jump distance, λ, according to $N = (R_{\mathrm{p}}/\lambda)^2$. If Φ is the Si interstitial dose, the number of hops per unit volume is $N \approx \Phi \cdot (R_{\mathrm{p}}/\lambda)^2 \cdot R_{\mathrm{p}}^{-1}$. Therefore, N is proportional to the dose and the distance to the surface. The temporary trapping of Si interstitials in immobile defects only delays their arrival to the surface, but not the total number of hops required to annihilate the defects.

An interesting issue concerning TED is the role of the temperature. In a dilute system and in the absence of traps, the diffusion length that a Bi travels before it breaks-up, and the B atom sits into a substitutional position and a Si interstitial moves away [55] is given by

$$\Gamma = \sqrt{6 \cdot D_{\mathrm{Bi}} \cdot \frac{1}{v_o} \cdot \exp\left(\frac{E^{\mathrm{Bi}}_{\mathrm{bind}} + E^{\mathrm{I}}_{\mathrm{m}}}{k_{\mathrm{B}}T}\right)} = \Gamma_0 \cdot \exp\left(-\frac{E_{\mathrm{act}}}{k_{\mathrm{B}}T}\right),$$

where Γ_0 is the prefactor, v_0 the vibrational frequency and $E_{\mathrm{act}} = (E^{\mathrm{Bi}}_{\mathrm{m}} - E^{\mathrm{Bi}}_{\mathrm{bind}} - E^{\mathrm{I}}_{\mathrm{m}})/2$, being $E^{\mathrm{Bi}}_{\mathrm{m}}$ the migration energy for the Bi diffusion. With the parameters typically used $E^{\mathrm{Bi}}_{\mathrm{m}} \sim 0.7$ eV, $E^{\mathrm{Bi}}_{\mathrm{bind}} \sim 1.0$ eV and $E^{\mathrm{I}}_{\mathrm{m}} \sim 1.0$ eV, it results $E_{\mathrm{act}} = -0.65$ eV. Although the individual parameters may not be precisely known, the activation energy can also be written as $E_{\mathrm{act}} = [(E^{\mathrm{I}}_{\mathrm{f}} + E^{\mathrm{Bi}}_{\mathrm{m}} - E^{\mathrm{Bi}}_{\mathrm{bind}}) - (E^{\mathrm{I}}_{\mathrm{f}} + E^{\mathrm{I}}_{\mathrm{m}})]/2$, being $E^{\mathrm{I}}_{\mathrm{f}}$ the formation energy of the Si interstitial from the ground state. The first term correspond to the activation energy for the equilibrium B diffusivity, and the second to the product $D_{\mathrm{I}} \cdot C^*_{\mathrm{I}}$, whose values are well established experimentally to be 3.5 and 4.8 eV, respectively [56,57]. The fact that the activation energy is negative implies that the total B diffusion length at the end of TED decreases as the temperature increases. At low temperatures or short annealing times, only a few B atoms have diffused long distances, giving rise to exponential profiles instead of the classical gaussian diffusing profiles resulting from the solution of the diffusion equation [54]. The fact that less TED occurs as the annealing temperature increases, has driven the trend to increase the annealing temperatures in Si processing ($T > 1000$ °C).

4.2. Dopant clustering

The analysis of B–I interaction in terms of the formation of a highly mobile pair is valid when the B concentration is low and all B atoms participate in TED. For high B concentrations, the formation of immobile and electrically inactive B complexes makes the problem more difficult [1,17]. Structures consisting of molecular beam epitaxy grown B marker layers implanted with Si ions were used to investigate the mechanisms of B clustering formation. In this type of structures the depth distribution of the mobile and immobile B components is clearly distinguished, as shown in Fig. 6. Important properties of the process can be extracted directly from a detailed analysis of this

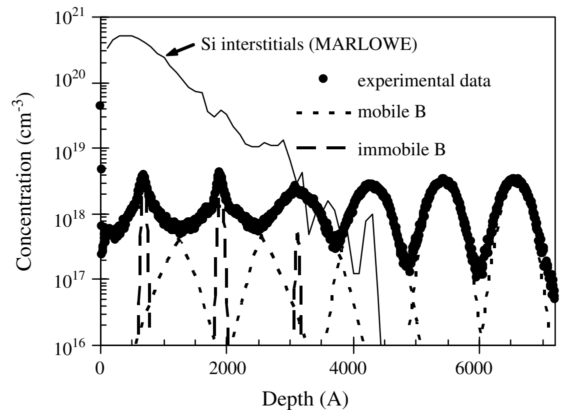

Fig. 6. SIMS profiles in B-doped superlattice after 40 keV, 5×10^{13} cm^{-2} Si implantation and 10 min anneal at 790 °C. The MARLOWE calculation of the initial Si interstitial distribution after implantation and the profile deconvolution into mobile and inmobile parts are also represented.

experiment [17]: (i) immobile B regions are observed only in the region that experiences very high Si interstitial supersaturation during implantation. This indicates that a Si interstitial rich defect is required to nucleate B clusters. (ii) The clustered component of B shows no broadening from the as-grown profile. This implies that a fraction of B atoms must be immobilized before any B diffusion occurs, i.e., during the room temperature implantation or at a very early stage of the annealing. In addition, no significant number of new nucleation sites can be formed once B starts diffusing; otherwise clustering would also take place outside of the initial spikes. (iii) All of the spikes, even the deepest ones, experience TED. Analogously, other experiments have shown that for B concentrations $\leqslant 10^{20}\,\mathrm{cm}^{-3}$ B clusters are formed only when the implant damage overlaps the B profile [18,58,59]. When the majority of Frenkel pairs has recombined, and more stable Si interstitial clusters have formed, the Si interstitial supersaturation set by these clusters causes TED but it is not enough to nucleate new B clusters. Since these B cluster precursors are formed before interstitial–vacancy recombination, the "+1" model, that successfully predicts TED, is not applicable to the modeling of B cluster formation.

The model for B clustering includes a complex pathway for B/Si interstitial interactions leading to B_nI_m complexes (B_nI_m represents a B cluster with n B atoms and m Si interstitials) responsible for B deactivation [18], as shown in the scheme of Fig. 7. The fact that the experimental data show no increase of the clustered B fraction during TED, but a slight reduction, indicates that large B clusters are unstable or that an energy barrier prevents their formation. For this reason only B clusters of small size are considered in the model. Still, the large number of equations involved in this mechanism makes its implementation in continuum models difficult. Some attempts have been made in that respect by considering only a reduced number of complexes [60,61]. The pathways for the B cluster formation and dissolution are determined by cluster energies and by B and Si interstitial concentrations. Fig. 8 represents the B cluster fraction for the combination of high and low B concentrations and high and low Si interstitial

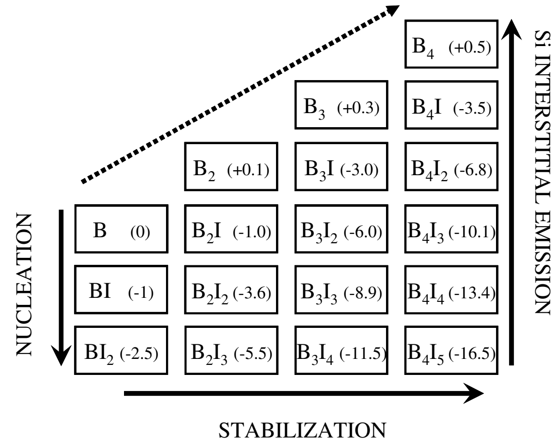

Fig. 7. Total energy of B clusters (in eV) considering the isolated B and Si interstitials as the energy reference (0 level) and schematic of the different paths for the growth of B clusters. The dashed line corresponds to a generic low interstitial content path. The solid line corresponds to a high interstitial content path.

concentrations, obtained by KMC simulations. Two main pathways can be identified: a low Si interstitial content pathway and a high Si interstitial content pathway [18]. In the low interstitial content path, the B cluster formation occurs through the capture of mobile Bi by the pre-existing clusters and the rapid release of Si interstitials, leaving B clusters with low interstitial content. In the high interstitial content path, Si interstitials are not emitted rapidly, resulting in B clusters rich in Si interstitials. Those interstitials are released later in the annealing, when the Si interstitial supersaturation decreases.

Empirical parameter extraction [17,18,62] and theoretical calculations [25,26] indicate that B clusters with no interstitials are energetically unfavourable ($E > 0$), while B clusters with interstitials are more stable (compared to separated B and Si interstitials). A bottleneck for the formation of B clusters through the low interstitial pathway must exist so that B clusters are not easily formed for medium B concentrations unless the Si interstitial concentration is high [18]. Theoretical calculations indicate that the energy of B_2 is quite high compared to that of Bi. Therefore, B_2I is more likely to dissolve into Bs+Bi than to form B_2 and release a Si interstitial. In the presence of large Si

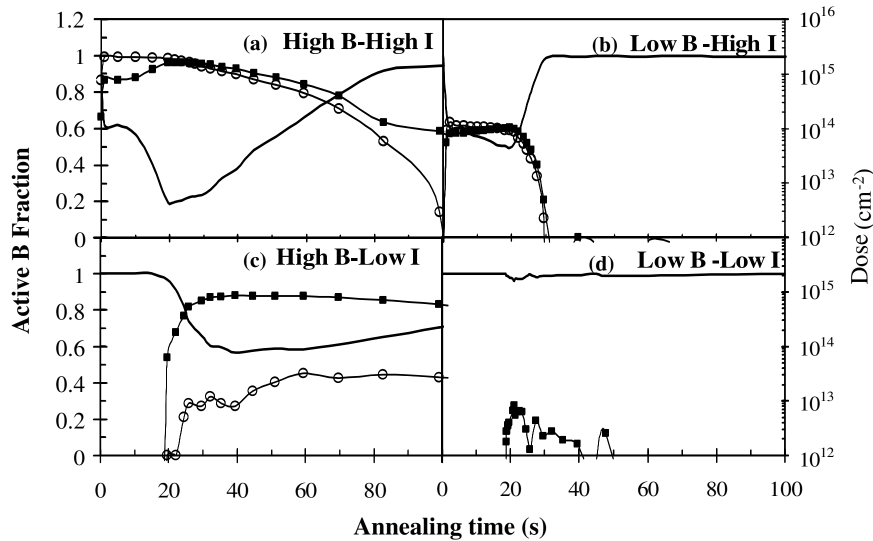

Fig. 8. Time evolution during annealing at 1000 °C (including the time for temperature ramp up at a rate of 50 °C/s) of the active B fraction (solid line), and the dose of B (closed symbols) and Si interstitials (open symbols) stored in B*n*I*m* clusters. (a) 10^{21} cm^{-3} B and I overlapping profiles; (b) 10^{20} cm^{-3} B and I overlapping profiles; (c) 10^{21} cm^{-3} B, no excess I; (d) 10^{20} cm^{-3} B, no excess I. When B and Si interstitial profile overlap, B clusters are formed. When there are no Si interstitials, B clusters are only formed in the case of high B concentration.

interstitial concentration, the formation of B clusters with high interstitial content (BI_2, B_2I_2, B_3I_3, B_4I_4) becomes the preferred pathway. In fact, experiments have shown that the B cluster formation acts as a trap for Si interstitials [59,63]. B clusters with high Si interstitial content are maintained while a Si interstitial supersaturation exists. When the Si interstitial supersaturation decreases, B clusters emit Si interstitials, resulting in low Si interstitial content B clusters that dissolve through the low interstitial content pathway. The existence of a Si interstitial supersaturation for longer time, for instance by annealing in an oxidizing ambient [64] or by the injection of Si interstitials from the EOR defects [65], retards the Si interstitial emission from B clusters and therefore, its dissolution.

When no excess Si interstitials overlap the B profile, the formation energy of Si interstitials must be taken into account in the evaluation of the total energy required for the B cluster formation. Because of the high Si interstitial formation energy, B clusters with a high interstitial content become an energetically unfavourable pathway. Since B clusters with low interstitial content are highly unstable, they are not nucleated outside regions that experience high Si interstitial supersaturation. However, when the initial B concentration is very high ($\geqslant 10^{21}$ cm^{-3}), B clusters can also form though the low interstitial content pathway. If the B concentration is very high, the initial interaction that forms B_2I can be driven toward B_2 and the release of a Si interstitial. Thus, B clusters can nucleate with minimal intervention of Si interstitials [62].

5. Conclusions

We have analyzed physically based models for ion implantation and annealing, including the evolution of Si interstitial defects and their interaction with B atoms to cause B diffusion and clustering. This study requires a multi-scale modeling: ab initio and MD calculations provide parameters and interactions to KMC and continuum simulators. Because of the atomistic nature of KMC codes, this method is more appropriate to capture local inhomogeneities, such as those resulting in the collision cascades. This effect has been also evidenced by statistical analysis of small devices [66]. When

the complexity of the model requires the use of a large number of differential equations, as it occurs for B-Si interstitial clusters, KMC methods are more efficient. As the device sizes are reduced and more complicated effects play a significant role, atomistic models appear more necessary in process simulations.

Acknowledgements

The authors would like to acknowledge the support, encouragement and fruitful discussions with George Gilmer, Hans Gossmann, John Poate and all the members of the party room at Bell Laboratories. This work has been partially supported by the Spanish DGICYT under project BFM 2001-2250 and the JCYL Consejería de Educación y Cultura under project VA-010/02.

References

[1] P.A. Stolk, H.-J.G.D.J. Eaglesham, D.C. Jacobson, C.S. Rafferty, G.H. Gilmer, M. Jaraiz, J.M. Poate, H.S. Luftman, T.E. Haynes, J. Appl. Phys. 81 (1997) 6031.
[2] International Technology Roadmap for Semiconductors, Available from: <http://public.itrs.net>.
[3] L. Csepregi, E.F. Kennedy, J.W. Mayer, T.W. Sigmon, J. Appl. Phys. 49 (1978) 3906.
[4] E. Landi, A. Armigliato, S. Solmi, R. Köghler, E. Wieser, Appl. Phys. A 47 (1998) 359.
[5] K.S. Jones, K. Moller, J. Chen, M. Puga-Lambers, B. Freer, J. Berstein, L. Rubin, J. Appl. Phys. 81 (1997) 6051.
[6] R. Lindsay, B. Pawlak, J. Kittl, K. Henson, C. Torregiani, S. Giangrandi, R. Surdeanu, W. Vandervorst, A. Mayur, J. Ross et al., Mater. Res. Soc. Symp. Proc. 765 (5) (2003) D7.4.1.
[7] J.-Y. Jin, J. Liu, U. Jeong, S. Mehta, K. Jones, J. Vac. Sci. Technol. B 20 (2002) 422.
[8] L. Pelaz, L.A. Marqués, M. Aboy, J. Barbolla, Defect Diffusion Forum (2003).
[9] K.B. Winterbon, P. Sigmund, J.B. Sanders, K. Dan Vidensk, Selsk. Mat. Fys. Medd. 37 (1970) 14.
[10] J.F. Ziegler, Stopping and Ranges of Ions in Matter, vol. 1, Pergamon, New York, 1977.
[11] M.T. Robinson, I.M. Torrens, Phys. Rev. B 9 (1974) 5008.
[12] P. Sigmund, Rev. Roum. Phys. 17 (1972) 823.
[13] G.H. Gilmer, T. Díaz de la Rubia, D.M. Stock, M. Jaraiz, Nucl. Instrum. Methods B 102 (1995) 247.
[14] T. Díaz de la Rubia, G.H. Gilmer, Phys. Rev. Lett. 74 (1995) 2507.
[15] M.J. Caturla, T. Díaz de la Rubia, L.A. Marqués, G.H. Gilmer, Phys. Rev. B 54 (1996) 16683.
[16] M. Jaraíz, G.H. Gilmer, T. Díaz de la Rubia, Appl. Phys. Lett. 68 (1996) 409.
[17] L. Pelaz, M. Jaraiz, G.H. Gilmer, H.-J. Gossmann, C.S. Rafferty, D.J. Eaglesham, J.M. Poate, Appl. Phys. Lett. 70 (1997) 2285.
[18] Pelaz, G.H. Gilmer, H.-J. Gossmann, J.M. Poate, C.S. Rafferty, M. Jaraiz, J. Barbolla, Appl. Phys. Lett. 74 (1999) 3657.
[19] M.E. Law, S.M. Cea, Comput. Mater. Sci. 12 (1998) 289.
[20] C. Rafferty, R.K. Smith, Comput. Model. Eng. Sci. 1 (2000) 151.
[21] J. Zhu, T. Díaz de la Rubia, L.H. Yang, C. Mailhiot, G.H. Gilmer, Phys. Rev. B 54 (1996) 4741.
[22] B. Shadigh, T.J. Lenosky, S.K. Theiss, M.-J. Caturla, Phys. Rev. Lett. 83 (1999) 4341.
[23] W. Windl, M.M. Bunea, R. Stumpf, S.T. Dunham, M.P. Masquelier, Phys. Rev. Lett. 83 (1999) 4345.
[24] P. Alippi, L. Colombo, P. Ruggerone, A. Sieck, G. Seifert, T. Frauenheim, Phys. Rev. B 64 (2001) 075207.
[25] T.J. Lenosky, B. Sadish, S.K. Theiss, M.J. Caturla, T. Díaz de la Rubia, Appl. Phys. Lett. 77 (2000) 1834.
[26] X.Y. Liu, W. Windl, M.P. Masquelier, Appl. Phys. Lett. 77 (2000) 2018.
[27] C.S. Rafferty, G.H. Gilmer, M. Jaraiz, D. Eaglesham, H.J. Gossmann, Appl. Phys. Lett. 68 (1996) 2395.
[28] G. Hobler, L. Pelaz, C.S. Rafferty, Nucl. Instrum. Methods B 153 (1999) 172.
[29] M.L. Swanson, J.R. Parsons, C.W. Hoelke, Radiat. Eff. 9 (1971) 249.
[30] F.F. Morehead, B.L. Crowder, Radiat. Eff. 6 (1970) 27.
[31] L. Pelaz, L.A. Marques, M. Aboy, J. Barbolla, G.H. Gilmer, Appl. Phys. Lett. 82 (2003) 2038.
[32] L.A. Marques, L. Pelaz, J. Hernandez, J. Barbolla, G.H. Gilmer, Phys. Rev. B 64 (2001) 45214.
[33] L.A. Marques, L. Pelaz, M. Aboy, L. Enrquez, J. Barbolla, Phys. Rev. Lett. 91 (2003) 135504.
[34] M. Tang, L. Colombo, J. Zhu, T.D. de la Rubia, Phys. Rev. B 55 (1997) 14279.
[35] D.M. Stock, B. Weber, K. Gärtner, Phys. Rev. B 61 (2000) 8150.
[36] M. Giles, J. Electrochem. Soc. 138 (1991) 1160.
[37] L. Pelaz, G.H. Gilmer, M. Jaraiz, S.B. Herner, H.-J. Gossmann, D.J. Eaglesham, G. Hobler, C.S. Rafferty, J. Barbolla, Appl. Phys. Lett. 73 (1998) 1421.
[38] L. Pelaz, G.H. Gilmer, V.C. Venezia, H.-J. Gossmann, M. Jaraiz, J. Barbolla, Appl. Phys. Lett. 74 (1999) 2017.
[39] G. Hobler, L. Pelaz, C.S. Rafferty, J. Electroc. Soc. 147 (2000) 3494.
[40] D.K. Sadana, M. Strathman, J. Washburn, G.R. Booker, J. Appl. Phys. 51 (1980) 5718.
[41] E. Lampin, V. Senez, A. Claverie, J. Appl. Phys. 85 (1999) 8137.
[42] G. Hobler, G. Otto, Mater. Sci. Semicond. Process. 6 (2003) 1.
[43] H. Cerva, G. Hobler, J. Electrochem. Soc. 139 (1992) 3631.

[44] A. Bongiorno, L. Colombo, F. Cargnoni, C. Gatti, M. Rosati, Europhys. Lett. 50 (2000) 608.
[45] D.J. Eaglesham, P.A. Stolk, H.J. Gossmann, J.M. Poate, Appl. Phys. Lett. 65 (1994) 2305.
[46] N.E.B. Cowern, G. Mannino, P.A. Stolk, F. Roozeboom, H.G.A. Huizing, J.G.M. van-Berkum, F. Cristiano, A. Claverie, M. Jaraiz, Phys. Rev. Lett. 82 (1999) 4460.
[47] I. Martin-Bragado, M. Jaraiz, P. Castrillo, R. Pinacho, J. Barbolla, M.M. de-Souza, Phys. Rev. B 68 (2003) 195204.
[48] F. Cristiano, J. Grisolia, B. Colombeau, M. Omri, B. de Mauduit, A. Claverie, L.F. Giles, N.E.B. Cowern, J Appl. Phys. 87 (2000) 8420.
[49] M. Aboy, L. Pelaz, L.A. Marqués, L. Enríquez, J. Barbolla, J. Appl. Phys. 94 (2003) 1010.
[50] A. Agarwal, T.E. Haynes, D.J. Eaglesham, H.J. Gossmann, D.C. Jacobson, J.M. Poate, Y.E. Erokhin, Appl. Phys. Lett. 70 (1997) 3332.
[51] H.J. Gossmann, T.E. Haynes, P.A. Stolk, D.C. Jacobson, G.H. Gilmer, J.M. Poate, H.S. Luftman, T.K. Mogi, M.O. Thompson, Appl. Phys. Lett. 71 (1997) 3862.
[52] J.S. Nelson, P.A. Schultz, A.F. Wright, Appl. Phys. Lett. 73 (1998) 247.
[53] P.M. Fahey, P.B. Griffin, J.D. Plummer, Rev. Mod. Phys. 61 (1989) 289.
[54] For example, Chapter 7 from D.R. Olander, Fundamental Aspects of Nuclear Reactor Fuel Elements, ERDA, Technical Information Center, Oak Ridge, TN, 1976.
[55] N.E.B. Cowern, G.F.A. van-de-Walle, D.J. Gravesteijn, C.J. Vriezema, Phys. Rev. Lett. 67 (1991) 212.
[56] R.B. Fair, J. Electroch. Soc. 137 (1990) 667.
[57] H. Bracht, E.E. Haller, R. Clark-Phelps, Phys. Rev. Lett. 81 (1998) 393.
[58] K.S. Jones, R.G. Elliman, M.M. Petravic, P. Kringhoj, Appl. Phys. Lett. 68 (1996) 3111.
[59] S. Solmi, L. Mancini, S. Milita, M. Servidori, G. Mannino, M. Bersani, Appl. Phys. Lett. 79 (2001) 1103.
[60] A.D. Lilak, S.K. Earles, K.S. Jones, M.E. Law, M.D. Giles, IEDM Techn. Dig. 493 (1997).
[61] S. Chakravarthi, S.T. Dunham, J. Appl. Phys. 89 (2001) 3650.
[62] M. Aboy, L. Pelaz, L.A. Marqués, J. Barbolla, A. Mokhberi, Y. Takamura, P.B. Griffin, J.D. Plummer, Appl. Phys. Lett. 83 (2003) 4166.
[63] T.E. Haynes, D.J. Eaglesham, P.A. Stolk, H.J. Gossmann, D.C. Jacobson, J.M. Poate, Appl. Phys. Lett. 69 (1996) 1376.
[64] L. Radic, A.D. Lilak, M.E. Law, Appl. Phys. Lett. 81 (2002) 826.
[65] M. Aboy, L. Pelaz, L.A. Marques, P. Lopez, J. Barbolla, R. Duffy, V. Venezia, P. Griffin, Appl. Phys. Lett. 86 (2005) 031908.
[66] A. Asenov, M. Jaraiz, S. Roy, G. Roy, F. Adamu-Lema, A.R. Brown, V. Moroz, R. Gafiteanu, SISPAD Proc. 87 (2002).